



## Research Article

# Application of NPZAD model to numerical study of biogeochemical parameters in the Persian Gulf

Akbarinia H.<sup>1</sup>; Ezam M.<sup>1\*</sup>; Ghavam Mostafavi P.<sup>1</sup>

Received: July 2021

Accepted: April 2022

### Abstract

A three-dimensional physical-biological numerical model namely ROMS was employed to investigate seasonal variations in biological parameters of Persian Gulf. The model domain included entire Persian Gulf and Sea of Oman. The model has run with climatic data. Lateral and surface boundary conditions were prepared from COADS and WOA09, respectively. The ROMS hydrodynamics model was coupled to bio-Fennel biological model including seven state variables (N2PChlZD2). After ten years' successive run, numerical results reached a quasi-steady-state and results of the tenth year were used for analysis. The model results revealed area of phytoplankton blooms and were in good consistency with surface chlorophyll data obtained from GMIS archive. The results showed two different peaks of chlorophyll growth in the region. The first peak occurred in spring in northwestern part of Persian Gulf where the blooms begin to grow up and expand to the middle and eastern parts of the region, and the second one occurred in late summer and early autumn in middle and southern parts. The results showed that the amount of chlorophyll in northwest and southern coastal waters was higher throughout the year in comparison to other parts of Persian Gulf, while in deep regions the role of eddies and residual currents are important in changing chlorophyll concentrations. In addition, the model showed that seasonal changes of biological parameters in Persian Gulf were nearly independent of Sea of Oman, and there was a significant relationship between biological parameters variations and seasonal changes of the region.

**Keywords:** Numerical modelling, Chlorophyll, Primary production, Persian Gulf

---

1-Marine Science Department, Faculty of Natural Resources and Environment, Science and Research Branch, Islamic Azad University, Tehran, Iran

\*Corresponding author's Email: ezam@srbiau.ac.ir

## Introduction

Today, concentration of atmospheric carbon dioxide and its impact on climate change has become one of the most important issues in the ecosystem. Oceans cover about 70% of the earth's surface and are largest carbon reservoirs of the Earth. They absorb carbon dioxide from the atmosphere and transport it in the form of organic and inorganic matters into deep water and control the amount of this gas in Earth's atmosphere through biogeochemical processes. It is estimated that they absorb about one-third of carbon dioxide produced by human activities and play an important role in physical and biological qualities of water systems. In addition, about 50% of total photosynthetic production of the Earth take places in oceans by providing food cycle of the ocean system.

In recent decades a wide range of ecosystem models with different capabilities has been developed to study the behavior of marine ecosystems. They investigate response of biological parameters to atmospheric and oceanic forcing. One of the relatively complex models is NPZD with several different state variables, including nutrients (N), phytoplankton (P), zooplankton (Z), and detritus (D). NPZD models can be simpler or more complex based on computational facilities, number, and diversity of the variables. Regarding its ability to give a real simulation, this model is used in many marine ecosystems, such as the comprehensive study in Bermuda (Fasham *et al.*, 1990), a study of biological parameters in North Atlantic with an emphasis on nitrogen

budget (Fennel *et al.*, 2006), applying EBUS sub-model for low-oxygen zone (Gutknecht *et al.*, 2013), a study of California Current System (Powell *et al.*, 2006), applying PISCES-V2 sub-model to calculate carbon budget (Aumont, 2005), and dozens of other studies.

In recent years a few in situ studies related to biological and chemical parameters of Persian Gulf and some modeling in Sea of Oman have been performed. For example, Sharifinia *et al.* (2015) and Rakib *et al.* (2021) investigated the amount of chlorophyll in several limited stations in Persian Gulf. Hamzei *et al.* (2012) used satellite data to study red tide that occurred in Persian Gulf in 2008, in the vicinity of northern Hormuz Strait. Lachkar *et al.* (2019) done some studies including the effect of warming of Persian Gulf on low oxygen zone in the Sea of Oman and its impact on primary production. Aberle and Piontkovski (2019) studied the dynamics of variability in microzooplankton in Sea of Oman. Moreover, Sedigh Marvasti *et al.* (2016) conducted studies of seasonal changes of phytoplankton in northwestern Arabian Sea and Gulf of Oman by employing coupled physical and biological models. Significantly, these studies resulted in the report of 66 cases of red tides between 1976 and 2004, which were associated with death of fish and aquatic organisms.

Persian Gulf is not only important in the view of ecological and economical systems but also has unique geographical conditions. Persian Gulf (PG) is located between 24-30 N and 48-56.5 E as shown in Figure 2. Its average depth is about 40

meters and its maximum depth is about 120 meters near Strait of Hormuz, which connects PG to Sea of Oman. Annual precipitation in the region is very low and is estimated to be about 15 centimeters. The amount of evaporation is high and is about 1.5 - 2 meters per year (Chao *et al.*, 1992). It is observed that PG has an annual water loss of about 416 cubic kilometers, most of which is due to high evaporation that is offset through Strait of Hormuz by Indian Ocean Surface Water, IOSW (Emery, 1956). Temperature of IOSW is about 26-23°C in winter and about 30-32°C in summer with a salinity of 36.5-37.2 PSU (Pous *et al.*, 2004). The maximum salinity is in the shallow southern coasts, reaching about 57 PSU (Ezam *et al.*, 2010). In eastern part of Gulf, IOSW plays an important role in shaping surface circulation of PG. The main branch of this current, under the influence of wind along the coast of Iran (51°E) in spring and summer, forms a current called Iranian Coastal Current (ICC), which has a velocity of about 20-30 cm/s, and other branches under the impact of Ekman drift northwesterly winds shifts to the south. In summer, ICC is destabilized to a mid-scale barotropic current known as Iran Coastal Eddies (ICE), which has saline and cold cores relative to the surrounding waters (Abdelrahman and Ahmad, 1995). Therefore, in winter due to cold weather and weaker wind, and reduced layering, the main circulation is weaker and only one cyclonic circulation prevails in the eastern basin, which is

much weaker than its summer circulation. (Pous *et al.*, 2013).

As mentioned above, recent studies of Persian Gulf mainly focused on dynamics and physical characteristics of water bodies. The basin circulations and major currents of the region are almost known. But biological parameters of this region, and effects of basin hydrodynamics and atmospheric forces on variation of these parameters have been less concerned. Accordingly in this research, an attempt is made to simulate and study seasonal changes in biological parameters of Persian Gulf using the coupled physical-biological ROMS<sup>1</sup> model. For this purpose, different parts of this research are presented as follows: First a brief introduction of ROMS numerical model and details of its biological equations are presented, secondly steps of the model preparation and execution are briefly described, and finally some of the major findings of the model and comparison with satellite altimetric data are discussed.

### Materials and methods

We used a coupled physical-biological ROMS model to predict seasonal changes of some biological parameters over Persian Gulf due to physical forces. ROMS is a new generation ocean circulation model (Shchepetkin and McWilliams, 2005) that is specially designed for accurate simulations of regional oceanic systems. It is a split-explicit, free-surface ocean model, where short time steps are used to advance the

---

<sup>1</sup> - Regional Ocean Modeling System

surface elevation and barotropic momentum, with a much larger time step used for temperature, salinity, and baroclinic momentum. The model can solve Reynolds-averaged Navier–Stokes equations using hydrostatic and Boussinesq assumptions, in Cartesian coordinates on horizontal, and sigma coordinates in the vertical direction. The model offers various ecosystem sub-models for ecological complexities (Haidvogel *et al.*, 2008).

#### *Physical model configuration*

The study area was Persian Gulf, which has three closed land borders and one open water border. Considering the effects of open boundary conditions in numerical models, open border has been extended to the end of Sea of Oman. We used ROMS for three-dimensional time-dependent oceanographic currents governed by hydrostatic primitive equations, with a local closure scheme, based on level 2.5 turbulent kinetic energy equations of Mellor and Yamada (Haidvogel *et al.*, 2008). Horizontal resolution of the model grid was 1/20 degrees with dimensions of approximately 4.99 km (less than the Rossby radius), and in vertical direction with 15 layers' grid using Sigma coordinate system. Also, time step was determined by considering the Courant number (CLF) for baroclinic and barotropic modes. Sea level was calculated by considering the initial

value  $SSHA=0$  with presence of tides. For this purpose, eight main components of the tide have been included in the model from the TMD model. Topographic data was also taken from ETOPO1<sup>1</sup> archive. The data required for surface forcing was provided from COADS<sup>2</sup> climatological data archive, which has a collection of atmospheric data of the entire globe with spatial resolutions of one degree. The data required for boundary conditions, including horizontal and vertical velocities, salinity, and surface temperature at open border of the model was prepared from WOA2009<sup>3</sup> archive, which provides climatic data on an average monthly basis at 1° resolution. Also, we used SeaWiFS<sup>4</sup> data for surface chlorophyll climatology dataset. To compare the results of the model with satellite data, global surface chlorophyll with accuracy of 4 km resolution was obtained from GMIS<sup>5</sup> archive and after performing some corrections values for the study region were extracted and used. First, the model was run for ten years with the mentioned climatic forcing and, finally results of the tenth year were used for analysis.

#### *Biological model components*

The biological model used in this study was adapted from Fennel *et al.* (2006). It was an expression of nitrogen cycle in aquatic basins and included seven state variables (N2PChlZD2), phytoplankton

<sup>1</sup> - 1 arc-minute global relief model of Earth's surface

<sup>2</sup> - Comprehensive Ocean-Atmosphere Data Set

<sup>3</sup> - World Ocean Atlas

<sup>4</sup> - Sea-Viewing of Wide Field-of-View Sensor

<sup>5</sup> - Global Marine Information System

(Phy), zooplankton (Zoo), nitrate (NO<sub>3</sub>), ammonium (NH<sub>4</sub>), chlorophyll-phytoplankton (Chl), small detritus (SDet), and large detritus (LDet). The

relation between these variables is depicted in Figure 1 (Fennel *et al.*, 2006).

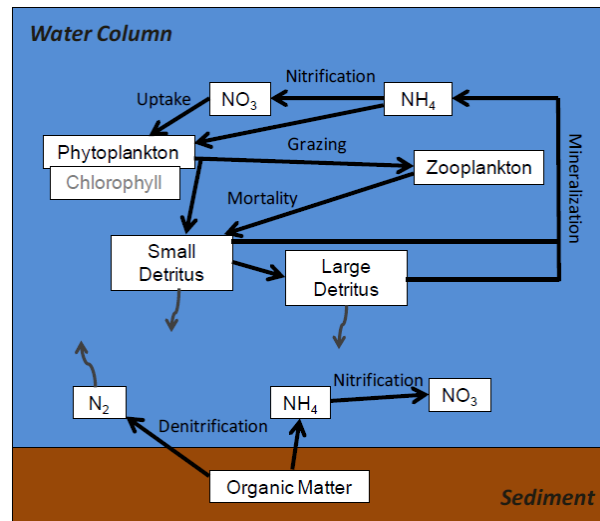


Figure 1: Schematic diagram of the Fennel biogeochemical model (Gillanders *et al.*, 2015).

In these processes, it was assumed that large-scale primary production, i.e., part of primary production that is supplied by arrival of nutrients from outside was equal to the amount of production that leaves the euphotic zone (Fasham *et al.*, 1990). The mixed layer is biologically homogeneous, which means that the rate of physical mixing in this layer is faster than the rate of growth of its organic matter (Eppley and Peterson, 1979). Use of nitrogen as a limiting nutrient causes primary production to be divided into a

new product that consumes nitrate, and a secondary product that uses mainly ammonium (Dugdale and Wilkerson, 1991), with advantages of calculation of f-ratio between these new and secondary productions (Fasham *et al.*, 1990). The mathematical relations are given in the following section.

*Phytoplankton*

The relation of temporal changes for phytoplankton is:

$$\frac{\partial Phy}{\partial t} = \mu \cdot Phy - g \cdot Zoo - m_p \cdot Phy - \tau(SDet + Phy)Phy - W_p \frac{\partial Phy}{\partial z} \tag{1}$$

In this relation,  $\mu$  is growth rate of phytoplankton and its value depends on temperature, and here this dependence is expressed based on the Apple relation as follows (Eppley, 1972):

$$\mu_{max} = \mu_{max}(T) = \mu_0 \cdot 1.066^T \tag{2}$$

$$\mu = f(I) \cdot (L_{NO3} + L_{NH4}) \tag{3}$$

$$L_{NH4} = \frac{NH4}{NH4 + K_{NH4}} \tag{4}$$

$$L_{NO3} = \frac{NO3}{NO3 + K_{NO3}} \times \frac{K_{NH4}}{NH4 + K_{NO4}} \tag{5}$$

The relations  $L_{NO_3}$  and  $L_{NH_4}$  are expressed here using the Michaelis-Menten equation for nitrate and ammonium, and express the limitation of nutrient uptake (Kirk, 1983). It is hypothesized that there is an inhibition of nitrate uptake in the presence of ammonium, which is expressed according to Parker (1993). Also  $K_{NH_4}$  and  $K_{NO_3}$  are coefficients of half-saturation concentration for ammonium and nitrate absorption, respectively.

$$I = I(Z) = I_0 \cdot PAR \cdot \exp\{-Z(K_w + K_{Chl})\} \quad (6)$$

Where  $I_0$  is the amount of light intensity just below the water surface, which is determined by latitude and day length in each season, PAR just below the water surface is also a function of the light available for photosynthesis. Also,  $K_w$  and  $K_{Chl}$  are light attenuation coefficients in the water column for water and chlorophyll respectively and are assumed to be constant with varying depths:

$$f(I) = \frac{\alpha \cdot I}{\sqrt{\mu_{max}^2 + \alpha^2 \cdot I^2}} \quad (7)$$

Where  $\alpha$  is initial slope of the curve (P-I),  $m_p$ ,  $w_p$  and  $\tau$  respectively are mortality, sinking velocity, and aggregation coefficient respectively.

$$\frac{\partial Chl}{\partial t} = \rho_{Chl} \cdot \mu \cdot Chl - g \cdot Zoo \frac{Chl}{Phy} - m_p \cdot Chl - \tau(SDet + Phy)Chl \quad (9)$$

$$\rho_{Chl} = \frac{\Theta_{max} \cdot \mu \cdot Phy}{\alpha \cdot I \cdot Chl} \quad (10)$$

Where  $\Theta_{max}$  is maximum chlorophyll to phytoplankton ratio (Geider *et al.*, 1997).

### Zooplankton

In this model, diversity of zooplankton is ignored and they are all placed in one

$$g = g_{max} \frac{Phy^2}{K_p + Phy^2} \quad (8)$$

Also  $g_{max}$  is maximum grazing rate of zooplankton from phytoplankton and  $K_p$  is half-saturated concentration in this grazing.

Here the mixed layer equation was not explicitly modeled, but it is assumed that seasonal change of the state variable (M) in depth of the mixed layer is mathematically a function of time (Fasham *et al.*, 1990):  $\frac{dM}{dt} = h(t)$ . By substituting the time variable according to velocity and depth of the mixed layer it yields:

$$W \frac{dM}{dz} = h(t)$$

### Chlorophyll

Relationship between chlorophyll of biomass and phytoplankton is nonlinear because the amount of chlorophyll in phytoplankton cell changes with the amount of photosynthetic active radiation and the amount of nutrient available to adapt to the environment with a wide range of carbon to chlorophyll ratio (C: Chl-a = 6-333) (Falkowski *et al.*, 1985):

herbivore category, and it is assumed that zooplankton converts their grazing of phytoplankton into their biomass with a coefficient of efficiency  $\beta$ , and transfer the remaining part  $1 - \beta$  to source of small detritus:

$$\frac{\partial Zoo}{\partial t} = g \cdot \beta \cdot Zoo - L_{BM} \cdot Zoo - L_E \cdot \frac{Phy^2}{K_p + Phy^2} \cdot \beta - m_z \cdot Zoo^2 \quad (11)$$

Other terms related to reduction of zooplankton, include two forms of ammonium excretion due to zooplankton metabolism and sloppy grazing with linear rates of  $L_{BM}$  and  $L_E$  respectively. Mortality term in the form of  $m_z \cdot Zoo^2$  also includes natural mortality or hunting or any other form of reduction in number that is proportional to the square of zooplankton biomass (Fennel *et al.*, 2006).

$$\frac{\partial SDet}{\partial t} = g(1 - \beta) \cdot Zoo + m_z \cdot Zoo^2 + m_p \cdot Phy - \tau(SDet + Phy)SDet - r_{SD} \cdot SDet - W_S \frac{\partial SDet}{\partial z} \quad (12)$$

$$\frac{\partial LDet}{\partial t} = \tau(SDet + Phy^2) - r_{LD} \cdot LDet - W_L \frac{\partial LDet}{\partial z} \quad (13)$$

Where  $r_{SD}$  and  $r_{LD}$  are mineralization rates for small and large detritus and  $W_S$  and  $W_L$  are sinking velocity of small and large detritus, respectively. Rapid sinking of detritus reduces the amount of decomposition to DIC<sup>1</sup> near the water surface, which directly affects the concentration of DIC, leading to a change in carbon dioxide pressure ( $p^{CO_2}$ ) and in carbon to chlorophyll ratio (Scott *et al.*, 2011).

$$\frac{\partial NH_4}{\partial t} = -\mu_{max} \cdot f(I) \cdot L_{NH_4} \cdot Phy - n \cdot NH_4 + L_{BM} \cdot Zoo + L_E \frac{Phy^2}{K_p + Phy^2} \beta \cdot Zoo + r_{SD} \cdot SDet + r_{LD} \cdot LDet \quad (15)$$

### *Small and Large Detritus*

Detritus are substances that are formed from deposition of zooplankton excretion, phytoplankton and zooplankton mortality, zooplankton nutrient residues, and of which a large part decomposed and returned in the form of dissolved organic matter to the cycle of nutrients required for primary production and are considered as follows:

### *Nitrate and Ammonium*

The relation between nitrate and ammonium changes is based on their biological processes as follows:

$$\frac{\partial NO_3}{\partial t} = -\mu_{max} \cdot f(I) \cdot L_{NO_3} \cdot Phy + n \cdot NH_4 \quad (14)$$

The first term shows NO<sub>3</sub> reduction equation due to phytoplankton uptake and the second sentence assumes that part of ammonium is nitrated at the rate of  $n$  and added to NO<sub>3</sub> source of water:

<sup>1</sup> - Dissolved Inorganic Carbon

The first two terms show taking up of phytoplankton from ammonium and reduction of ammonium due to nitrification, respectively. The second and third terms are related to excretion of ammonium by zooplankton due to their nutrition or metabolism. The last two terms are related to respiration of detritus by  $r_{SD}$  and  $r_{LD}$  rates, that the nitrification

rate  $n$ , is expressed by the following relation (Olson, 1981):

$$n = n_{max} \left\{ 1 - \max \left( 0, \frac{I - I_0}{K_I + I - I_0} \right) \right\} \quad (16)$$

Biological parameters used in the model are listed in Table 1. More detail information about parameter values can be found in Fennel *et al.* (2006).

**Table 1: List of parameters used in the biogeochemical model.**

Symbol	Parameter	Value	Unit
$\mu_0$	phytoplankton growth rate at 0°C	2.9	d <sup>-1</sup>
$K_{NO3}$	half-saturation concentration for uptake of NO <sub>3</sub>	0.5	mmolNO <sub>3</sub> m <sup>-3</sup>
$K_{NH4}$	half-saturation concentration for uptake of NH <sub>4</sub>	0.5	mmolNO <sub>3</sub> m <sup>-3</sup>
$\alpha$	The initial slope of the P-I curve	0.025	(wm <sup>-2</sup> d) <sup>-1</sup>
$g_{max}$	maximum grazing rate	0.6	d <sup>-1</sup> mmolNO <sub>3</sub> m <sup>-3</sup>
$K_p$	half-saturation concentration of phytoplankton ingestion	2	mmolNO <sub>3</sub> m <sup>-3</sup>
$m_p$	phytoplankton mortality	0.15	d <sup>-1</sup>
$\tau$	aggregation parameter	0.005	d <sup>-1</sup> mmolNO <sub>3</sub> m <sup>-3</sup>
$\Theta_{max}$	maximum chlorophyll to phytoplankton ratio	0.053	mgChl(mgC) <sup>-1</sup>
$\beta$	assimilation efficiency	0.75	-
$L_{BM}$	excretion rate due to basal metabolism	0.1	d <sup>-1</sup>
$L_E$	maximum rate of assimilation related excretion	0.1	d <sup>-1</sup>
$m_z$	zooplankton mortality	0.025	d <sup>-1</sup> mmolNO <sub>3</sub> m <sup>-3</sup>
$r_{SD}$	remineralization rate of suspended detritus	0.03	d <sup>-1</sup>
$r_{LD}$	remineralization rate of large detritus	0.01	d <sup>-1</sup>
$n_{max}$	maximum nitrification rate	0.05	d <sup>-1</sup>
$K_I$	light intensity at which inhibition of nitrification is half-saturated	0.1	wm <sup>-2</sup>
$I_0$	The threshold for light-inhibition of nitrification	0.0095	wm <sup>-2</sup>
$W_p$	sinking velocity of phytoplankton	0.01	md <sup>-1</sup>
$W_{SDet}$	sinking velocity of suspended detritus	0.01	md <sup>-1</sup>
$W_{LDet}$	sinking velocity of large detritus	1	md <sup>-1</sup>

## Results

The results of the model over Persian Gulf along with a cross-section (DE path as shown in Figure 2) are presented for two months. For September when phytoplankton blooms, and for December when primary production declines. In addition, to show temporal changes of biological parameters, the

time series at three selective points located at north-west (point A), south (point B) and east of Persian Gulf (point C) are illustrated. Geographic locations of the points are shown in Figure 2, and first in Figures 3-4 patterns of monthly changes of chlorophyll are examined.

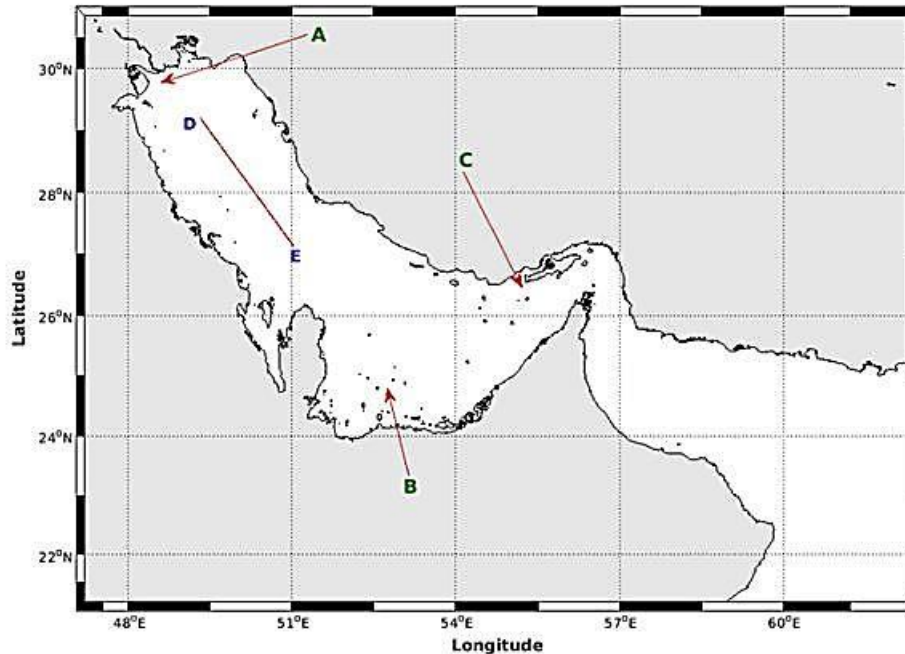


**Figure 2:** Geographical location of Persian Gulf and Oman Sea; and A, B and C points located in 48.5°E-29.5°N, 52.5°E - 25°N and 55.3°E - 26.7°N respectively; and vertical cross-section along DE line from 49.5°E, 29°N to 51°E, 27°N.

According to mean monthly patterns and time series of surface chlorophyll changes (Figs. 3-4) It is predicted that the two regions can be separated according to an expansion of surface chlorophyll. In northwestern region, blooms begin in spring and extend along southern coasts and center of Persian Gulf, and come down to a minimum in winter. In central and eastern parts, chlorophyll growth begins in late summer and peaks in fall,

and continues until early winter. Figure 4 also shows a large difference in maximum amount of chlorophyll in location A ( $5 \text{ mgChlm}^{-3}$ ) compared to B and C locations (around  $0.12 \text{ mgChlm}^{-3}$  and  $0.1 \text{ mgChlm}^{-3}$  respectively), and their temporal peaks in northwest occur in spring, and for other regions in late summer and early autumn.

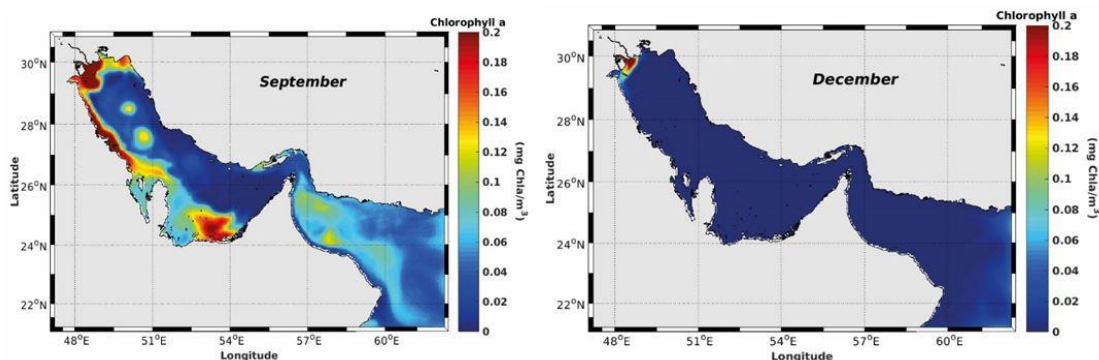


**Figure 3:** Mean monthly surface chlorophyll concentrations in Persian Gulf and Sea of Oman in September and December.

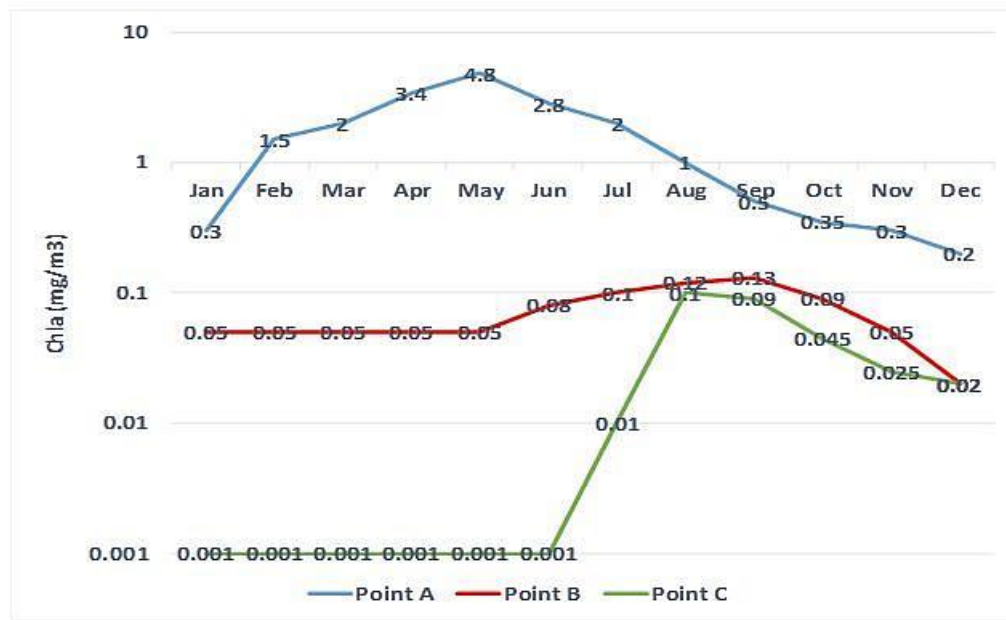


Figure 4: Mean monthly values of chlorophyll concentrations in locations A, B, and C.

To outline the effects of eddy activities on distribution of biological variables with depths, in Figure 5 cross-sections of chlorophyll in September and December are shown. During September due to presence of cyclonic eddies (as can be seen in Figure 15), there is an increase in chlorophyll where cyclonic eddies cause

water particles to pump upwards and hence, increase transfer of nutrients from depth to euphotic zone. During December due to weakening of the eddies, primary production has been stopped and chlorophyll concentration rapidly decreases.

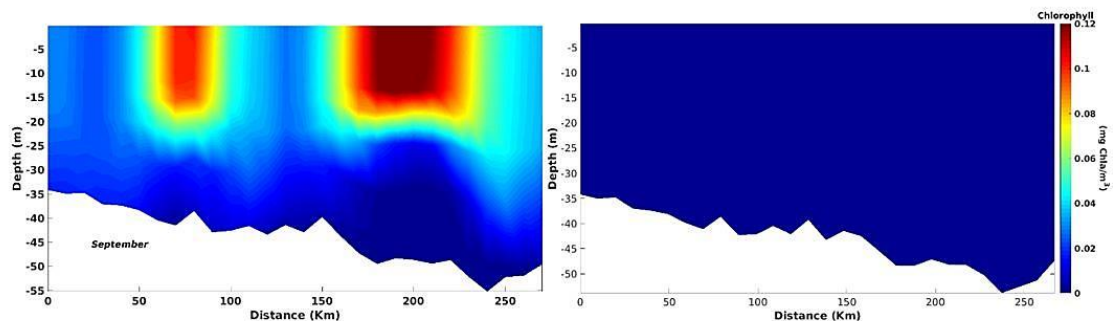


Figure 5: Vertical chlorophyll concentrations in the DE cross-section in September and December, respectively.

Mean monthly phytoplankton concentrations for September and December are shown in Figure 6. As expected, a good similarity between phytoplankton and chlorophyll concentrations is observed.

The time series of phytoplankton concentrations at the three mentioned points are presented in Figure 7 showing the differences in amount and temporal peaks of phytoplankton during the year. Figure 8 shows vertical concentrations of

phytoplankton along the DE cross-section. At the location of the two eddies, similar to chlorophyll, phytoplankton concentration reached its maximum

values expanding to a depth of 20 to 30 meters in September and disappeared in December.

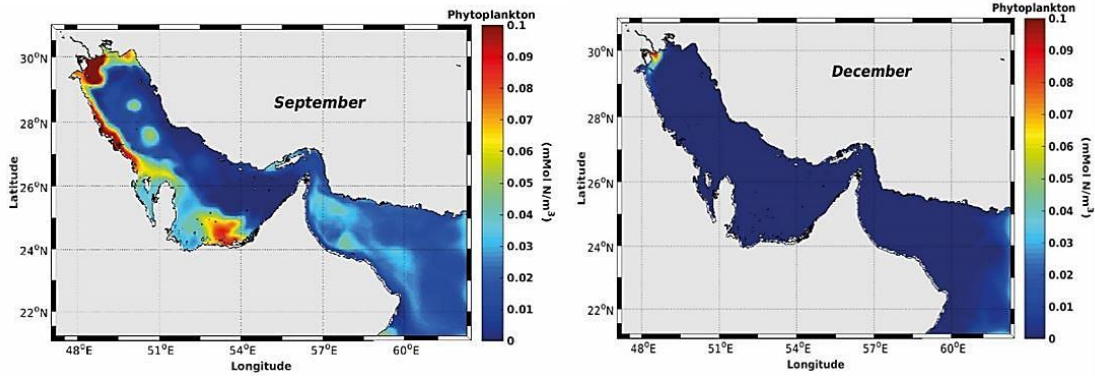


Figure 6: Monthly pattern of phytoplankton distribution in Persian Gulf and Sea of Oman in September and December.

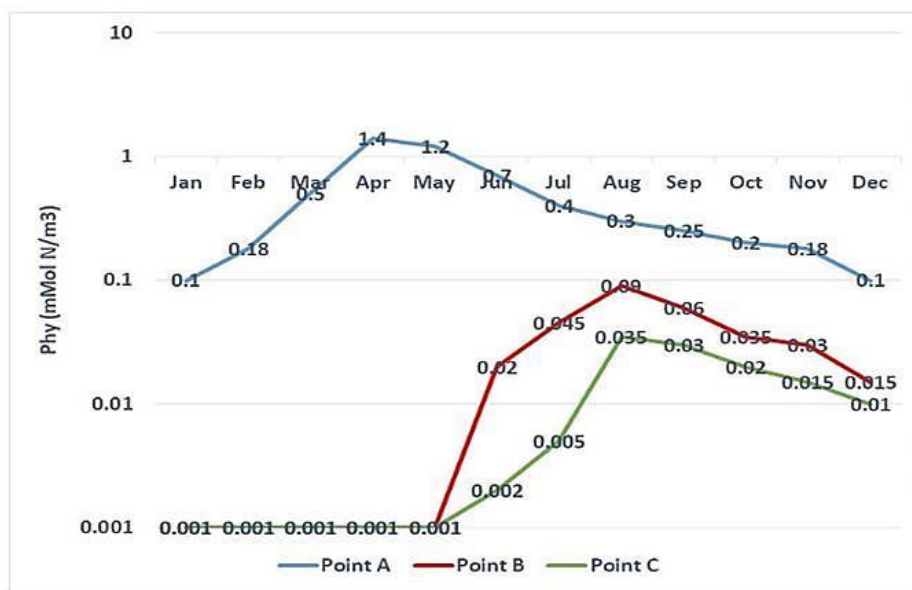


Figure 7: Mean monthly values of phytoplankton concentrations in locations A, B, and C.

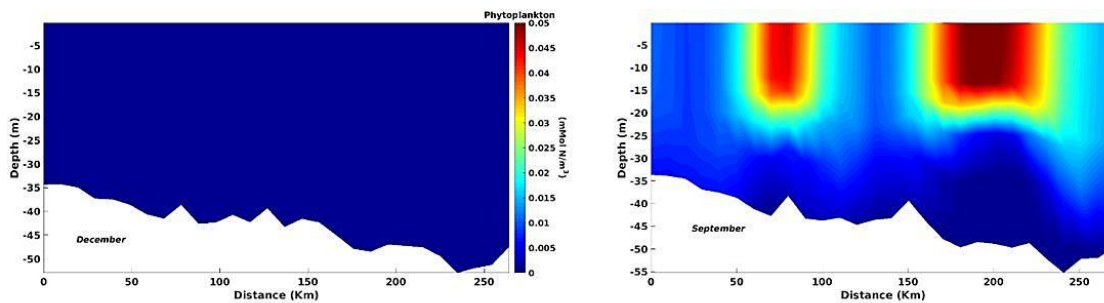


Figure 8: Vertical phytoplankton distribution in the DE cross-section in September and December, respectively.

Figures 9-10 are patterns of mean monthly surface nitrate, and its vertical distribution in September and December, respectively, along the DE cross-section region. It is clear that in areas of high chlorophyll and phytoplankton concentrations, due to consumption of nitrate for primary production the amount of nitrate is getting inversely decreased. In addition, the amount of nitrate in places of the cyclonic eddies,

where the highest amount of primary production has occurred, is the lowest ones. Figure 10 shows that the amount of nitrate increases with depth and is getting decreased only where primary production occurs. Thus, importance of baroclinic currents and cyclonic eddies which may lead to upwelling and pumping nutrients from the bed to euphotic zone is concluded.

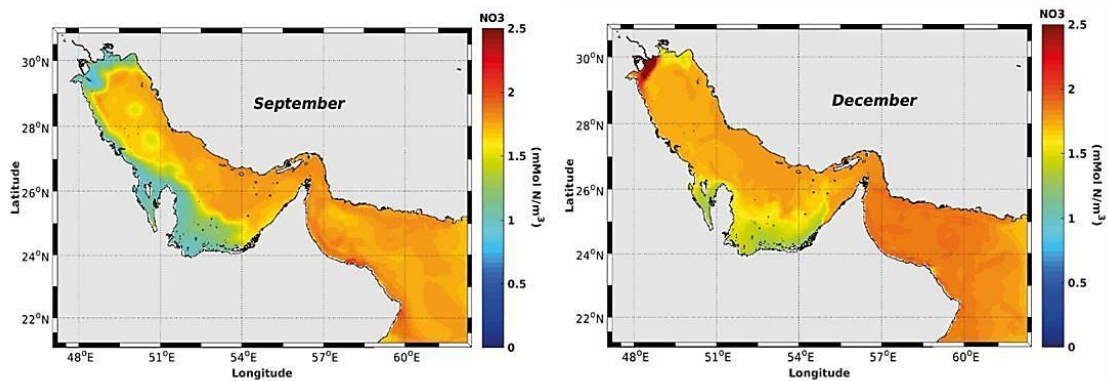


Figure 9: Monthly pattern of surface nitrate in Persian Gulf and Sea of Oman in September and December.

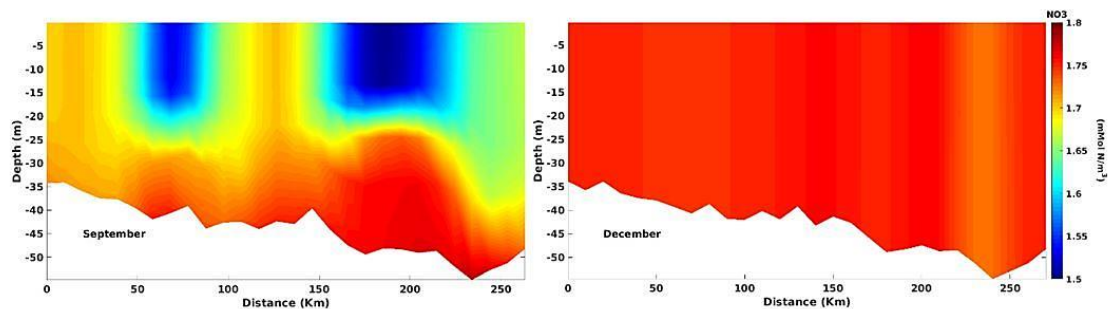


Figure 10: Vertical nitrate concentrations along the DE cross-section region in September and December.

Figure 11 shows time series of nitrate concentrations in A, B, and C locations and reveals that in late autumn and winter the amount of nitrate in northern part of Persian Gulf has its maximum annual values of about  $6 \text{ mmol Nm}^{-3}$  in location A compared to less than  $2 \text{ mmol Nm}^{-3}$  in B and C locations. From early summer the amount of nitrate on

southern coasts begins to decline rapidly, which is due to high nitrate consumption and phytoplankton blooms. As a whole, during the year in middle and east parts of Persian Gulf, nitrate concentrations are less than that of northwestern parts, which lead to less primary production in these regions.

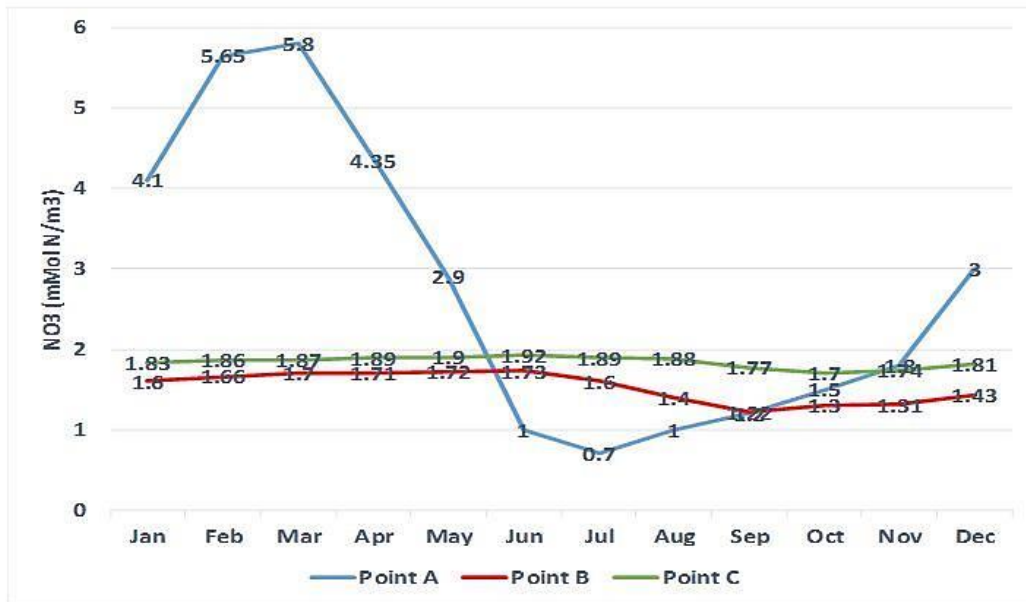


Figure 11: Mean monthly values of nitrate in A, B, and C locations.

In case of ammonium (NH<sub>4</sub>) Figures 12 to 14 are presented. Figure 12 shows monthly concentration of ammonium at the surface for September and December respectively. Ammonium is mostly a product of zooplankton excretion and detritus decomposition and its distribution pattern is similar to those of phytoplankton. Figure 13 shows the pattern of vertical concentrations of ammonium along the DE cross-section in September and December. The time

series of monthly values of ammonium in A, B, and C locations are shown in Figure 14, showing that in the northwestern regions (point A) the ammonium concentration is higher relative to other areas of the Gulf. It peaks at about 0.5  $mmol Nm^{-3}$  in late spring and early summer (June) and reaches its minimum values in early winter.

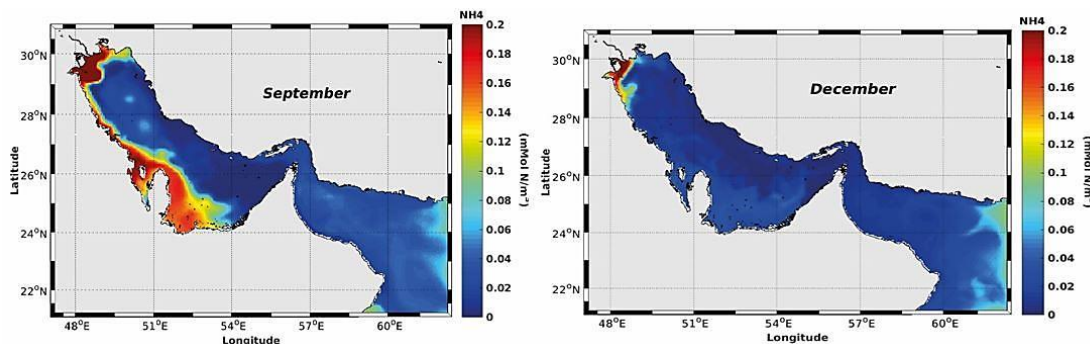


Figure 12: Monthly pattern of surface ammonium concentrations in Persian Gulf and Sea of Oman in September and December.

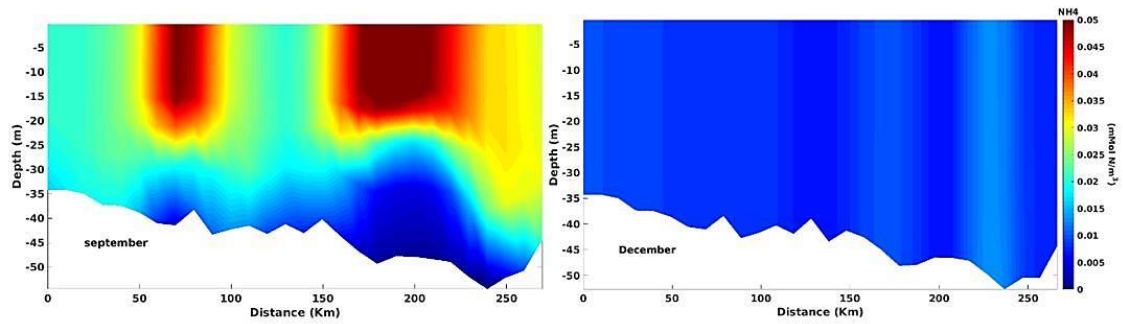


Figure 13: Vertical concentrations of ammonium (NH<sub>4</sub>) along the DE path for September and December.

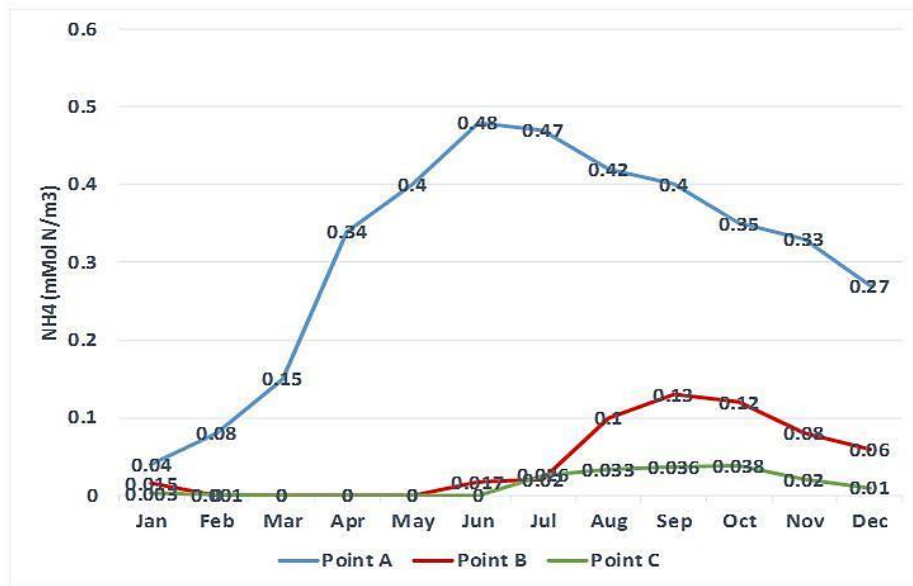


Figure 14: Mean monthly values of ammonium concentration in A, B, and C locations.

Figures 15-16 show mean monthly of velocity field and cross-section of current speed along DE path for September and December respectively,

to represent locations and depths of influence of major eddies along DE path and to investigate their effects on other variables.

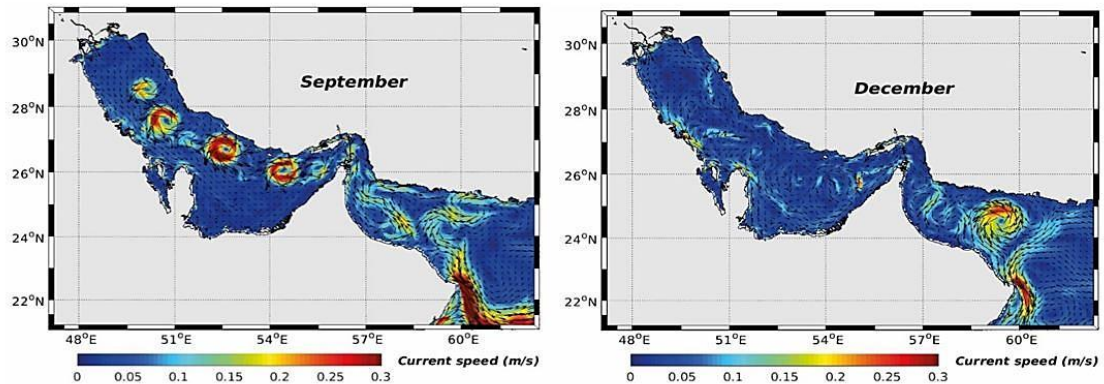
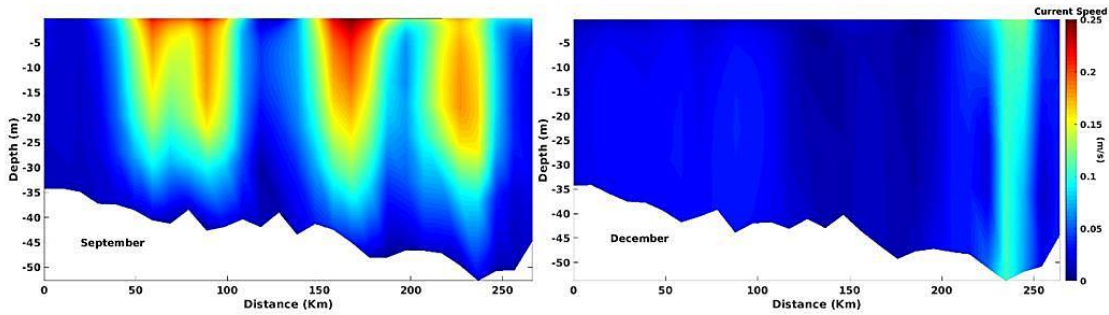


Figure 15: Mean monthly of velocity field in Persian Gulf and Sea of Oman in September and December.



**Figure 16: Vertical distribution of current speed along DE cross-section in September and December.**

Cross-sections of temperature filed in Figure 17 conform that during September formation of cyclonic eddies in shallow depths influenced almost entire water column. As a result, nearly cold and nutritious water adjacent to the

sea bottom is pumped upwards. Intruding these waters in the mixed layer and euphotic zone provide favorable conditions for phytoplankton bloom to occur.

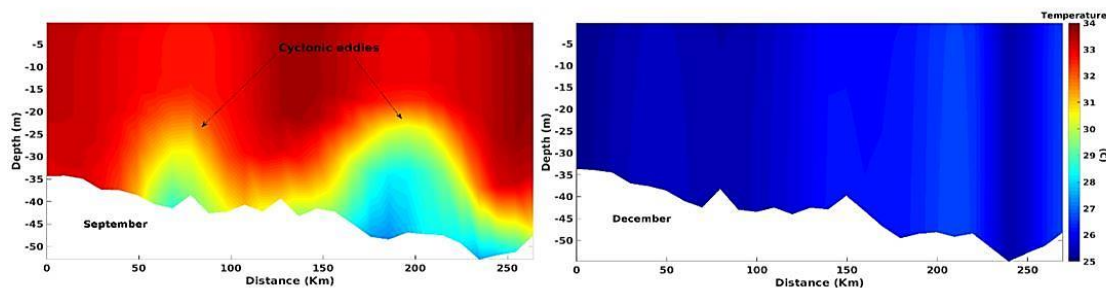


**Figure 17: Temperature cross-sections along DE path during September and December. Arrows show temperature upwelling due to two cyclonic eddies in September.**

## Discussion

Circulations of water in Persian Gulf are influenced by many factors, such as wind stress at the surface, buoyancy and thermocline forces, and tides which lead to forming small-scale and mesoscale eddies. The main barotropic cycle, which occurs between June and August includes a cyclonic eddy in southeast of this basin and an anticyclone eddy in northwest. They break up into smaller eddies from July to October. The ICC flows in spring and summer in northern part of Persian Gulf from Strait of Hormuz to north of Qatar at a speed of

about 20-30 cm/s and includes some mesoscale eddies with a diameter of about 115-130 km that covers all depth of the water. Meanwhile, in summer with instability of ICC and forming the ICE, mesoscale barotropic currents with saline and cold-core relative to surrounding waters form, and bring necessary nutrients for primary production from depth to the surface and increase the depth of mixed layer as well. When wind intensifies an upwelling along the coast of Iran and downwelling along the coast of Arabian countries form and stratification decreases. In winter this

structure is replaced with smaller structures and the currents are more affected by the wind pattern. In western basin, northern currents continue along Arvand River forming a small gyre and carrying saline water of shallow coasts near Qatar and joining mainstream in central part of Persian Gulf. As they feed the PGW through Strait of Hormuz, they create a fertile region for primary production 36 along their path.

To validate results of the model, we extracted the surface Chlorophyll data over the study area from GMIS archive with resolutions of 4 km. After making some necessary corrections, monthly basin averaged surface chlorophyll over Persian Gulf and Sea of Oman for 12-years period from 2005 to 2017 was calculated and shown in Figures 18-19.

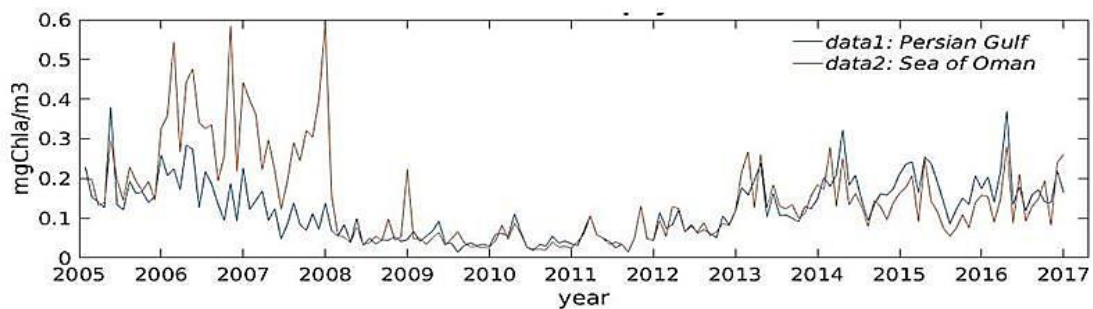


**Figure 18: Monthly basin averaged surface chlorophyll over Persian Gulf and Sea of Oman for 2005-2017.**

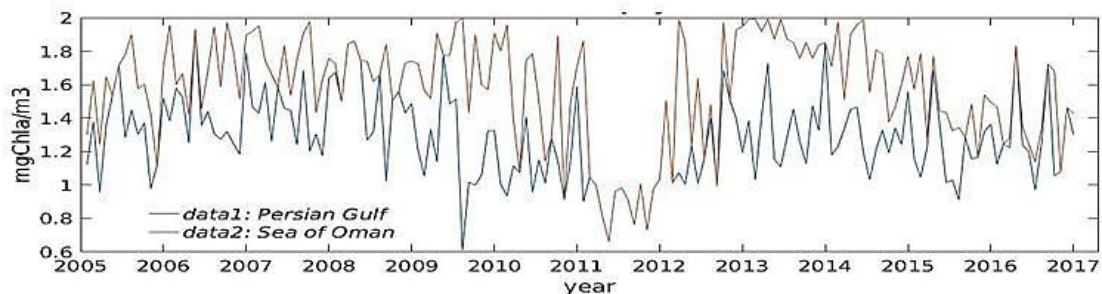


**Figure 19: Maximum mean monthly surface chlorophyll over Persian Gulf and Sea of Oman for 2005-2017.**

As can be concluded from Figures 18-19, monthly average surface chlorophyll obtained from satellite databases in both Persian Gulf and Sea of Oman during these years has an average of about  $0.2 \text{ mgChlm}^{-3}$  and maximum of about  $2 \text{ mgChlm}^{-3}$ . These values show a good consistency with the results obtained from the present model in the climatic run. It's worth noting that the default

NPZD model which is included in the ROMS, generally yields underestimated values of surface chlorophyll for the study area. So, we had to do many successive runs to yield the best configuration for the model parameters which was beyond the scope of this paper.

It should be noted again that available previous research in Persian Gulf did not

provide information about the maximum amount of chlorophyll, especially in offshore waters; however, the study of Harrison *et al.* (2018) in Arabian Sea has shown that two peaks of chlorophyll blooms occur during the year. One from August to September at the end of South West Monsoon (SWM), and another from February to March when North East Monsoon (NEM) has terminated. In that study, the highest chlorophyll amount in Sea of Oman is estimated to be less than  $2 \text{ mgcm}^{-3}$  during NEM, and less than  $1 \text{ mgcm}^{-3}$  during SWM. Rakib *et al.* (2021) measured the amount of chlorophyll in some stations close to Qatar with values of about  $0.81 \text{ mgChlm}^{-3}$  and  $0.68 \text{ mgChlm}^{-3}$  that is close to our results in that region. Furthermore, the modeling results of Sedigh Marvasti *et al.* (2016) at Sea of Oman shown that the maximum amount of chlorophyll in the region was about  $1.5\text{-}2 \text{ mgChlm}^{-3}$  which is compatible with the results of our model results.

The model results revealed that seasonal changes of surface chlorophyll in Persian Gulf behave nearly independent of Oman Sea in climatic view. In Persian Gulf, growth of surface chlorophyll begins from northwest and extends to the east and southern shallow areas. It seems that this evolution could be justified appropriately by the pattern of permanent wind and hydrodynamics of Persian Gulf. In addition, this study follows the results of Al-Azri *et al.* (2012) which concluded that growth of phytoplankton blooms begins in Persian

Gulf and then it is transferred to Sea of Oman with currents.

Regarding relative independence of phytoplankton growth of Persian Gulf from Sea of Oman, it is referred to consequences of storms that carry a lot of specks of dust into Persian Gulf and cause increase in metallic nutrients such as iron that enrich chlorophyll growth and intensify the blooms (Anwar *et al.*, 1986). Das and Mishra (2013) also concluded that after most dust storms there is an increase in chlorophyll amount and it is a sign of limited iron nutrients in the region. Therefore, strength of dust storms and increase of metallic nutrients can be considered as one of the potential drivers of productivity in oceanic water. It's necessary to say that in our model we did not take into account effects of dust transmitted by storms. Moreover, the results showed that the amount of surface chlorophyll in the shallow water on northwest and southern coasts of Persian Gulf is relatively high during the entire year in comparison to other areas.

A survey on satellite measurements of surface chlorophyll at a glance showed a significant increase in average amount of chlorophyll from 2006 to 2008, which peaked in Sea of Oman at  $0.6 \text{ mgChlm}^{-3}$  and reached about  $0.3 \text{ mgChlm}^{-3}$  in Persian Gulf, which is related to red tide phenomenon that occurred in that time. Figures 18-19 show that from 2013 to 2016 the average amount of chlorophyll in Persian Gulf slightly exceeded that in Sea of Oman. Excluding the values of some northwestern coastal regions that showed

high levels of chlorophyll, the maximum amount of chlorophyll was about  $2 \text{ mgChlm}^{-3}$  in both Persian Gulf and Sea of Oman.

Monsoon winds are another atmospheric phenomenon that can lead to fertility of the region and affect dynamics of phytoplankton growth, especially in Oman Sea, as mentioned by Harrison *et al.* (2018). In General, the intensity of NEM is weaker than SWM, but because it occurs with decreasing surface water temperature in winter, it increases water mixing rate and depth of the mixed layer as well. Along with upwelling due to wind stress which brings up nutrients from the depth, an increase in chlorophyll and phytoplankton bloom occurs and continues until spring. This also happens at the time of SWM, with the difference that surface water is warmer than deep water and upwelling brings colder water and nutrients from depths to the surface and increases primary production. In this case, Reynolds (1993) argued that the effect of NEM causes an upwelling near the coast of Iran and fertilizes the area. Also other phenomena, such as mixing, advection, pumping and Ekman transport, mesoscale eddies due to local winds also play an important role in providing required nutrients to increase productivity or transfer chlorophyll to other regions (Piontkovski *et al.*, 2011). To investigate seasonal changes in biological parameters of Persian Gulf, we implemented ROMS numerical hydrodynamic model coupled to a biological N2ChIPZD2 model. Initial and boundary conditions of the model

were prepared from a set of different global archives. We evaluated the model results with global surface chlorophyll values obtained from GMIS archive. Furthermore, the model results were examined with different ranges for parameters to yield the appropriate values for biological parameters of the model for Persian Gulf.

The model results indicated that surface chlorophyll of Persian Gulf begins to increase from northwestern part of Persian Gulf in spring and expands towards southern parts and blooms in late summer. It seems that the pattern of surface chlorophyll growth and its spreading in Persian Gulf is almost independent of that of Sea of Oman. Also, the results showed that the amount of chlorophyll in shallow waters of northwest and southern coasts is higher during the year in comparison to other parts. In addition, in the deep regions, role of meso-scale eddies and major currents are important to transport the concentrations. The results also showed that monthly average of surface chlorophyll of the region is less than  $0.3 \text{ mgChlm}^{-3}$  and without considering the values of small areas in coastal regions its monthly maximum reaches to about  $2 \text{ mgChlm}^{-3}$ .

In this study only nitrate was considered as the primary production and limiting nutrient, further studies are recommended to take into account the role of other limiting nutrients, such as silicates, iron, phosphate, etc.

### Acknowledgments

We would like to thank developers of ROMS numerical model who provide and support the code to be freely available for researchers, as well as all the centers related to the World Oceanic and Atmospheric Data Archives.

### References

- Abdelrahman, S.M. and Ahmad, F., 1995.** A note on the residual currents in the Arabian Gulf. *Continental Shelf Research*, 15(8), 1015-1022. [https://doi.org/10.1016/0278-4343\(95\)80006-y](https://doi.org/10.1016/0278-4343(95)80006-y).
- Aberle, N. and Piontkovski, S.A., 2019.** Seasonal dynamics of microzooplankton communities in the Sea of Oman (Arabian Sea). *Aquatic Ecosystem Health and Management*, 22(2), 131-140. <https://doi.org/10.1080/14634988.2019.1617002>.
- Al-Azri, A., Piontkovski, S., Al-Hashmi, K., Al-Gheilani, H., Al-Habsi, H., Al-Khusaibi, S. and Al-Azri, N., 2012.** The occurrence of algal blooms in Omani coastal waters. *Aquatic Ecosystem Health and Management*, 15(sup1), 56-63. <https://doi.org/10.1080/14634988.2012.672151>.
- Anwar, M., Gharib, I., Al-Hashash, M. and Zaghoul, N., 1986.** *Surface modelling of dust fallout on the ROPME Sea Area*. Annual research report -Kuwait Institute for Scientific Research, pp. 121-124.
- Aumont, O., 2005.** *PISCES biogeochemical model description*. Internal report, 36 P.
- Chao, S.Y., Kao, T.W. and Al-Hajri, K.R., 1992.** A numerical investigation of circulation in the Arabian Gulf. *Journal of Geophysical Research: Oceans*, 97(C7), 11219-11236. <https://doi.org/10.1029/92jc00841>.
- Das, B. and Mishra, A.K., 2013.** Effect of dust storm on phytoplankton productivity in Arabian Sea. *Journal of Remote Sensing and GIS*, 4(3), 33-44.
- Dugdale, R.C. and Wilkerson, F.P., 1991.** Low specific nitrate uptake rate: A common feature of high-nutrient, low-chlorophyll marine ecosystems. *Limnology and Oceanography*, 36(8), 1678-1688. <https://doi.org/10.4319/lo.1991.36.8.1678>.
- Emery, K.O., 1956.** Sediments and water of Persian Gulf. *AAPG Bulletin*, 40(10), 2354-2383. <https://doi.org/10.1306/5CEAE595-16BB-11D7-8645000102C1865D>.
- Eppley, R.W., 1972.** Temperature and phytoplankton growth in the sea. *Fishery Bulletin - National Oceanic and Atmospheric Administration*, 70(4), 1063-1085. [https://doi.org/10.1016/0278-4343\(95\)80006-y](https://doi.org/10.1016/0278-4343(95)80006-y).
- Eppley, R.W. and Peterson, B.J., 1979.** Particulate organic matter flux and planktonic new production in the deep ocean. *Nature*, 282(5740), 677-680. <https://doi.org/10.1038/282677a0>.
- Ezam, M., Bidokhti, A. A., and Javid, A. H., 2010.** Numerical simulations of spreading of the Persian Gulf outflow into the Oman Sea. *Ocean Science*,

- 6(4), 887-900.  
<https://doi.org/10.5194/os-6-887-2010>.
- Falkowski, P.G., Dubinsky, Z. and Wyman, K., 1985.** Growth-irradiance relationships in phytoplankton. *Limnology and Oceanography*, 30(2), 311-321.  
<https://doi.org/10.4319/lo.1985.30.2.0311>.
- Fasham, M.J.R., Ducklow, H.W. and McKelvie, S.M., 1990.** A nitrogen-based model of plankton dynamics in the oceanic mixed layer. *Journal of Marine Research*, 48(3), 591-639.  
<https://doi.org/10.1357/002224090784984678>.
- Fennel, K., Wilkin, J., Levin, J., Moisan, J., O'Reilly, J. and Haidvogel, D., 2006.** Nitrogen cycling in the Middle Atlantic Bight: Results from a three-dimensional model and implications for the North Atlantic nitrogen budget. *Global Biogeochemical Cycles*, 20(3).  
<https://doi.org/10.1029/2005GB002456>.
- Geider, R.J., MacIntyre, H.L. and Kana, T.M., 1997.** Dynamic model of phytoplankton growth and acclimation: responses of the balanced growth rate and the chlorophyll a: carbon ratio to light, nutrient-limitation and temperature. *Marine Ecology Progress Series*, 148(1-3), 187-200.  
<https://doi.org/10.3354/meps148187>.
- Gillanders, B., Goldsworthy, S.D., Prowse, T.A., Doubell, M., Middleton, J.F., Rogers, P.J., Tanner, J.E., Clisby Nathan, A., James, C.E., John, L. and Van Ruth, P., 2015.** Spencer Gulf Research Initiative: Development of an Ecosystem Model for Fisheries and Aquaculture. *Fisheries Research and Development Corporation*.  
 ??????pages ....
- Gutknecht, E., Dadou, I., Le Vu, B., Cambon, G., Sudre, J., Garçon, V., Machu, E., Rixen, T., Kock, A., Flohr, A., Paulmier, A. and Lavik, G., 2013.** Coupled physical/biogeochemical modeling including O<sub>2</sub>-dependent processes in the Eastern Boundary Upwelling Systems: application in the Benguela. *Biogeosciences*, 10(6), 3559-3591.  
<https://doi.org/10.5194/bg-10-3559-2013>.
- Haidvogel, D.B., Arango, H., Budgell, W.P., Cornuelle, B.D., Curchitser, E., Di Lorenzo, E., Fennel, K. et al., 2008.** Ocean forecasting in terrain-following coordinates: Formulation and skill assessment of the Regional Ocean Modeling System. *Journal of Computational Physics*, 227(7), 3595-3624.  
<https://doi.org/10.1016/j.jcp.2007.06.016>.
- Hamzei, S., Bidokhti, A.A., Mortazavi, M.S. and Gheibi, A., 2012.** Utilization of satellite imageries for monitoring harmful algal blooms at the Persian Gulf and Gulf of Oman. International Conference on Environmental, Biomedical and Biotechnology IPCBEE, 41, 171-174.
- Harrison, P., Piontkovski, S. and Al-Hashmi, K., 2018.** Overview of

- decadal ecosystem changes in the Western Arabian Sea and the occurrence of algal blooms. *Journal of Agricultural and Marine Sciences*, 23, 11-23. <https://doi.org/10.24200/jams.vol23iss0pp11-13>.
- Kirk, J.T.O., 1983.** Ecological strategies. In: *Light and photosynthesis in aquatic ecosystem*, Kirk, J.T.O., editor, 291-357. Cambridge University Press, Cambridge, UK. <https://doi.org/10.1002/iroh.19850700619>.
- Lachkar, Z., Lévy, M. and Smith, K.S., 2019.** Strong intensification of the Arabian Sea oxygen minimum zone in response to Arabian Gulf warming. *Geophysical Research Letters*, 46(10), 5420-5429. <https://doi.org/10.1029/2018GL081631>.
- Olson, R.J., 1981.** Differential photoinhibition of marine nitrifying bacteria: a possible mechanism for the formation of the primary nitrite maximum. *Journal of Marine Research*, 39(2), 227-238.
- Parker, R.A., 1993.** Dynamic models for ammonium inhibition of nitrate uptake by phytoplankton. *Ecological Modelling*, 66(1-2), 113-120. [https://doi.org/10.1016/0304-3800\(93\)90042-q](https://doi.org/10.1016/0304-3800(93)90042-q).
- Piontkovski, S., Al-Azri, A. and Al-Hashmi, K., 2011.** Seasonal and interannual variability of chlorophyll in the Gulf of Oman compared to the open Arabian Sea regions. *International Journal of Remote Sensing*, 32(22), 7703-7715. <https://doi.org/10.1080/01431161.2010.527393>.
- Pous, S.P., Carton, X. and Lazure, P., 2004.** Hydrology and circulation in the Strait of Hormuz and the Gulf of Oman—Results from the GOGP99 Experiment: 2. Gulf of Oman. *Journal of Geophysical Research: Oceans*, 109(C12), 57-78. <https://doi.org/10.1029/2003jc002146>.
- Pous, S., Carton, X.J. and Lazure, P., 2013.** A process study of the wind-induced circulation in the Persian Gulf. *Open Journal of Marine Science*, 3(1), 1-11. <https://doi.org/10.4236/ojms.2013.31001>.
- Powell, T.M., Lewis, C.V.W., Curchitser, E.N., Haidvogel, D.B., Hermann, A.J. and Dobbins, E.L., 2006.** Results from a three-dimensional, nested biological-physical model of the California Current System and comparisons with statistics from satellite imagery. *Journal of Geophysical Research: Oceans*, 111(C7). <https://doi.org/10.1029/2004jc002506>.
- Rakib, F., Al-Ansari, E.M.A.S., Husrevoglu, Y.S., Yigiterhan, O., Al-Maslmani, I., Aboobacker, V.M. and Vethamony, P., 2021.** Observed variability in physical and biogeochemical parameters in the central Arabian Gulf. *Oceanologia*, 63(2), 227-237. <https://doi.org/10.1016/j.oceano.2020.12.003>.

- Raynolds, R.M., 1993.** Physical oceanography of the Gulf, Strait of Hormuz, and the Gulf of Oman – Results from the Mt. Mitchell expedition. *Marine Pollution Bulletin*, 27, 35-59. [https://doi.org/10.1016/0025-326x\(93\)90007-7](https://doi.org/10.1016/0025-326x(93)90007-7).
- Scott, V., Kettle, H. and Merchant, C.J., 2011.** Sensitivity analysis of an ocean carbon cycle model in the North Atlantic: an investigation of parameters affecting the air-sea CO<sub>2</sub> flux, primary production and export of detritus. *Ocean Science*, 7(3), 405-419. <https://doi.org/10.5194/os-7-405-2011>.
- Sedigh Marvasti, S., Gnanadesikan, A., Bidokhti, A.A., Dunne, J.P. and Ghader, S., 2016.** Challenges in modeling spatiotemporally varying phytoplankton blooms in the Northwestern Arabian Sea and Gulf of Oman. *Biogeosciences*, 13(4), 1049-1069. <https://doi.org/10.5194/bg-13-1049-2016>.
- Sharifinia, M., Mohammadpour Penchah, M., Mahmoudifard, A., Gheibi, A. and Zare, R., 2015.** Monthly variability of chlorophyll- $\alpha$  concentration in Persian Gulf using remote sensing techniques. *Sains Malaysiana*, 44(3), 387-397.
- Shchepetkin, A.F. and McWilliams, J.C., 2005.** The regional oceanic modeling system (ROMS): a split-explicit, free-surface, topography-following-coordinate oceanic model. *Ocean Modelling*, 9(4), 347-404. <https://doi.org/10.1016/j.ocemod.2004.08.002>.